**Wind and Structures**, *Vol. 30, No. 2 (2020) 133-140*
DOI: https://doi.org/10.12989/was.2020.30.2.133


# Dynamic analysis of laminated nanocomposite pipes under the effect of turbulent in viscoelastic medium

M.M. Ghaitani, A. Majidian* and V. Shokri

*Department of Mechanical Engineering, Sari Branch, Islamic Azad University, Sari, Iran, P.O.B. 4816119318, Sari, Iran*

*(Received October 9, 2018, Revised September 22, 2019, Accepted September 30, 2019)*

**Abstract**. In this paper, critical fluid velocity and frequency of laminated pipe conveying fluid are presented. Each layer of the pipe is reinforced by functionally graded carbon nanotubes (FG-CNTs). The internal fluid is assumed turbulent and the induced forces are calculated by momentum equations. The pipe is resting on viscoelastic foundation with spring, shear and damping constants. The motion equations are derived based on classical shell theory and energy method. Differential quadrature method (DQM) is used for solution and obtaining the critical fluid velocity. The effects of volume percent and distribution of CNT, boundary condition, lamina layer number, length to radius ration of pipe, viscoelastic medium and fluid velocity are shown on the critical fluid velocity. Results show that with increasing the lamina layer number, the critical fluid velocity increases.

**Keywords:** critical fluid velocity; laminated pipeline; nanocomposite; turbulent internal fluid; viscoelastic foundation

## 1. Introduction

Carbon nanotubes has many applications in different industries due to the high hardness-to-weight and strength-to-weight ratios and other better properties compared with traditional isotropic ones. These structures can be used in aircraft, helicopters, missiles, launchers, satellites and etc. During the last 5 decades the application of sandwich structures with light core and two thin fasesheets have been extensively investigated.

There are many works in the literature for instability induced by fluid flow on different structures. Ryu *et al.* (2004) studied vibration and dynamic stability of cantilevered pipes conveying fluid on elastic foundations. Amabili (2008) studied vibration and stability of cylindrical shell conveying fluid using different theories. The instability of simply supported pipes conveying fluid under thermal loads was studied by Qian *et al.* (2009). A relatively new semi-analytical method, called differential transformation method (DTM), was generalized by Ni *et al.* (2011) to analyze the free vibration problem of pipes conveying fluid with several typical boundary conditions. Instability of supported pipes conveying fluid subjected to distributed follower forces was investigated by Wang (2012) based on the Pflüger column model. Marzani *et al.* (2012) investigated the effect of a non-uniform Winkler-type elastic foundation on the stability of pipes conveying fluid fixed at the upstream end only. The dynamics of fluid-conveying cantilevered pipe consisting of two segments made of different materials was studied by Dai and Ni (2013), focusing on the effects induced by different length ratios between the two segments. An analytical study of the velocity profile effects for a straight pipe was presented by Kutin and Bajsić (2014). A numerical simultaneous solution involving a linear elastic model was applied by Sun and Gu (2014) to study the fluid-structure interaction (FSI) of membrane structures under wind actions. The unsteady fluid-structure interaction (FSI) problems with large structural displacement were solved by He (2015) using partitioned solution approaches in the arbitrary Lagrangian-Eulerian finite element framework. Rivero-Rodriguez and Pérez-Saborid (2015) carried out a numerical investigation of the three dimensional nonlinear dynamics of a cantilevered pipe conveying fluid in the presence of gravity. Texier and Dorbolo (2015) described the deformation of an elastic pipe submitted to gravity and to an internal fluid flow. Maalawi *et al.* (2016) enhanced the pipe overall stability level and avoid the occurrence of flow. Ghaitani and Majidian (2017) addressed vibration and instability of embedded functionally graded (FG)-carbon nanotubes (CNTs)-reinforced pipes conveying viscous fluid. Structural model for a slender and uniform pipe conveying fluid, with axially moving supports on both ends, immersed in an incompressible fluid, was formulated by Ni *et al.* (2017). A hybrid method which combines reverberation-ray matrix method and wave propagation method was developed by Deng *et al.* (2017) to investigate the stability of multi-span viscoelastic functionally graded material (FGM) pipes conveying fluid.

Critical fluid velocity of the nanocomposite laminated pipes conveying fluid has not been investigated by any researcher. So in this research, for the first time, the critical fluid velocity response of the nanocomposite laminated pipe conveying turbulent fluid is studied based on classical theory of shell. Mixture method is used to evaluate the material properties of the nanocomposite. The viscosity and perturbation forces of the fluid are assumed by momentum equations. The critical fluid velocity of the structure is derived using DQM. In present study, effect of various

*Corresponding author, Associate Professor
E-mail: a_majidian@iausari.ac.ir


http://www.techno-press.com/journals/was&subpage=7
ISSN: 1226-6116 (Print), 1598-6225 (Online)

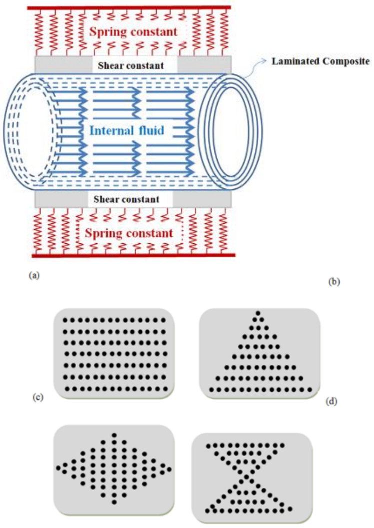


Fig. 1 Schematic of laminated nocomposite pipe conveying fluid embedded in viscoelastic medium

parameters like volume percent of CNTs, boundary conditions, geometrical parameters of pipe, internal fluid on the critical fluid velocity of the structure is presented.

## 2. Formulation

In Fig. 1, a laminated pipe conveying turbulent fluid flow embedded in viscoelastic medium is shown. Each layers of the pipe are reinforced by CNTs as functionally graded. The pipe has length of $L$, radius of $R$ and thickness of $h$.

Based on classical shell theory, the displacement fields of the pipe are (Amabili 2008)

$$u(x,\theta,z,t) = u(x,\theta,t) - z\frac{\partial w(x,\theta,t)}{\partial x}, \tag{1}$$

$$v(x,\theta,z,t) = v(x,\theta,t) - z\frac{\partial w(x,\theta,t)}{R\partial\theta}, \tag{2}$$

$$w(x,\theta,z,t) = w(x,\theta,t), \tag{3}$$

where $(u,v,w)$ are the middle displacements. The strain-displacement relations of the structure are

$$\begin{Bmatrix} \varepsilon_{xx} \\ \varepsilon_{\theta\theta} \\ \gamma_{x\theta} \end{Bmatrix} = \begin{Bmatrix} \varepsilon_{xx}^{0} \\ \varepsilon_{\theta\theta}^{0} \\ \gamma_{x\theta}^{0} \end{Bmatrix} - z\begin{Bmatrix} \varepsilon_{xx}^{1} \\ \varepsilon_{\theta\theta}^{1} \\ \gamma_{x\theta}^{1} \end{Bmatrix}, \tag{4}$$

Where

$$\begin{Bmatrix} \varepsilon_{xx}^{0} \\ \varepsilon_{\theta\theta}^{0} \\ \varepsilon_{x\theta}^{0} \end{Bmatrix} = \begin{Bmatrix} \dfrac{\partial u}{\partial x} + \dfrac{1}{2}\left(\dfrac{\partial w}{\partial x}\right)^2 \\ \dfrac{\partial v}{R\partial\theta} + \dfrac{w}{R} + \dfrac{1}{2}\left(\dfrac{\partial w}{R\partial\theta}\right)^2 \\ \dfrac{\partial v}{\partial x} + \dfrac{\partial u}{R\partial\theta} + \dfrac{\partial w}{\partial x}\dfrac{\partial w}{R\partial\theta} \end{Bmatrix}, \tag{5}$$

$$\begin{Bmatrix} \varepsilon_{xx}^{1} \\ \varepsilon_{\theta\theta}^{1} \\ \varepsilon_{x\theta}^{1} \\ \varepsilon_{xz}^{1} \\ \varepsilon_{\theta z}^{1} \end{Bmatrix} = \begin{Bmatrix} \dfrac{\partial^2 w}{\partial x^2} \\ \dfrac{\partial^2 w}{R^2\partial\theta^2} \\ \dfrac{2\partial^2 w}{R\partial\theta\partial x} \end{Bmatrix}, \tag{6}$$

Based on Hook law, the stresses of the pipe are

$$\begin{bmatrix} \sigma_{xx} \\ \sigma_{\theta\theta} \\ \tau_{x\theta} \end{bmatrix} = \begin{bmatrix} C_{11} & C_{12} & 0 \\ C_{21} & C_{22} & 0 \\ 0 & 0 & C_{66} \end{bmatrix} \begin{bmatrix} \varepsilon_{xx} \\ \varepsilon_{\theta\theta} \\ \gamma_{x\theta} \end{bmatrix}, \tag{7}$$

where the elastic constants of $E_{ij}$ can be obtained by Mixture rule as

$$E_{11} = \eta_1 V_{CNT} E_{r11} + (1 - V_{CNT}) E_m, \tag{8a}$$

$$\frac{\eta_2}{E_{22}} = \frac{V_{CNT}}{E_{r22}} + \frac{(1 - V_{CNT})}{E_m}, \tag{8b}$$

$$\frac{\eta_3}{G_{12}} = \frac{V_{CNT}}{G_{r12}} + \frac{(1 - V_{CNT})}{G_m}, \tag{8c}$$

where $E_{r11}$, $E_{r22}$ and $E_m$ are Young's moduli of CNTs and matrix, respectively; $G_{r11}$ and $G_m$ are shear modulus of CNTs and matrix, respectively; $V_{CNT}$ and $V_m$ show the volume fractions of the CNTs and matrix, respectively; $\eta_j$ (j= 1, 2, 3) is CNT efficiency parameter for considering the size-dependent material properties. Noted that this parameter may be calculated using molecular dynamic (MD). However, the CNT distribution for the mentioned patters obeys from the following relations

$$UD: \quad V_{CNT} = V_{CNT}^{*}, \tag{9a}$$

$$FGV: \quad V_{CNT}(z) = \left(1 + \frac{2z}{h}\right) V_{CNT}^{*}, \tag{9b}$$

$$FGO: \quad V_{CNT}(z) = 2\left(1 - \frac{2|z|}{h}\right) V_{CNT}^{*}, \tag{9c}$$

$$FGX: \quad V_{CNT}(z) = 2\left(\frac{2|z|}{h}\right) V_{CNT}^{*}, \tag{9d}$$

Noted that Poisson's ratio is assumed as constant. The potential energy can be written as

$$U = \int_V (\sigma_{xx}\varepsilon_{xx} + \sigma_{\theta\theta}\varepsilon_{\theta\theta} + \sigma_{x\theta}\gamma_{x\theta})\, dV, \tag{10}$$

By substituting strains into Eq. (10) yields

$$\begin{aligned} U = \int_A \Bigg( & N_x\left(\frac{\partial u}{\partial x} + 0.5\left(\frac{\partial w}{\partial x}\right)^2\right) - M_x\frac{\partial^2 w}{\partial x^2} + N_\theta\left(\frac{\partial v}{R\partial\theta} + \frac{w}{R} + 0.5\left(\frac{\partial w}{R\partial\theta}\right)^2\right) \\ & - M_\theta\frac{\partial^2 w}{R^2\partial\theta^2} + N_{x\theta}\left(\frac{\partial u}{R\partial\theta} + \frac{\partial v}{\partial x} + \frac{\partial w}{R\partial\theta}\frac{\partial w}{\partial x}\right) - 2M_{x\theta}\frac{\partial^2 w}{R\partial\theta\partial x}\Bigg) dA \end{aligned} \tag{11}$$

where the force and moment resultants are

$$\begin{Bmatrix} N_x \\ N_\theta \\ N_{x\theta} \end{Bmatrix} = \sum_{k=1}^{N} \int_{z^{(k-1)}}^{z^{(k)}} \begin{Bmatrix} \sigma_x \\ \sigma_\theta \\ \tau_{x\theta} \end{Bmatrix}^{(K)} dz\,, \tag{12}$$

$$\begin{Bmatrix} M_x \\ M_\theta \\ M_{x\theta} \end{Bmatrix} = \sum_{k=1}^{N} \int_{z^{(k-1)}}^{z^{(k)}} \begin{Bmatrix} \sigma_x \\ \sigma_\theta \\ \tau_{x\theta} \end{Bmatrix}^{(K)} z\,dz\,, \tag{13}$$

where $N$ in the number of layers. The kinetic energy may be expressed as

$$K = \frac{\rho}{2} \int_v \left( (\frac{\partial u}{\partial t})^2 + (\frac{\partial v}{\partial t})^2 + (\frac{\partial w}{\partial t})^2 \right) dV\,, \tag{14}$$

By substituting Eqs. (1) - (3) into (14) yields

$$K = \frac{1}{2} \int \left( \left( I_2 \left( (\frac{\partial^2 u}{\partial t\, \partial x})^2 + (\frac{\partial^2 w}{\partial t\, \partial \theta})^2 \right) \right) + I_0 \left( (\frac{\partial u}{\partial t})^2 + (\frac{\partial v}{\partial t})^2 + (\frac{\partial w}{\partial t})^2 \right) \right) dA\,, \tag{15}$$

Where

$$\begin{Bmatrix} I_0 \\ I_2 \end{Bmatrix} = \sum_{k=1}^{N} \int_{z^{(k-1)}}^{z^{(k)}} \begin{bmatrix} \rho \\ \rho z^2 \end{bmatrix}^{(K)} dz\,. \tag{16}$$

The external work due to viscoelastic medium is

$$W_v = \int_A \left( -k_w w + k_g \nabla^2 w - c_v \left[ \frac{\partial w}{\partial t} \right] \right) w dA, \tag{17}$$

where $k_w$, $k_g$ and $c_v$ are spring, shear and damp constants of viscoelastic foundation. In a fully developed turbulent pipe flow, the momentum equations are (Reddy 2004, Amabili 2008)

$$\frac{1}{\rho_e} \frac{\partial P}{\partial x} = -\frac{1}{r} \frac{\partial}{\partial r} \left( r \bar{v}_x \bar{v}_r \right) + \frac{\mu_e}{r \rho_e} \frac{d}{dr} \left( r \frac{dv_x}{dr} \right), \tag{18}$$

$$\frac{1}{\rho_e} \frac{\partial P}{\partial r} = -\frac{1}{r} \frac{\partial}{\partial r} r \left( \bar{v}_r \right)^2 + \frac{\left( \bar{v}_\theta \right)^2}{r}, \tag{19}$$

$$0 = -\frac{\partial}{\partial r} \bar{v}_\theta \bar{v}_r - \frac{2 \bar{v}_r \bar{v}_\theta}{r}, \tag{20}$$

where $\bar{v}_r, \bar{v}_\theta, \bar{v}_x$ are the turbulent fluctuating velocity components in the $r$, $\theta$ and $x$ directions, respectively; $\mu_e$ is the fluid viscosity. After lengthy mathematical manipulations, the pressure in the r and x directions can be expressed as

$$P_r = 2 \frac{\rho_e}{R} U_\tau^2 L\,, \tag{21}$$

$$P_x = \rho_e U_\tau^2\,, \tag{22}$$

where $U\tau$ is the shear velocity which can be given as

$$U_\tau^2 = \left( \frac{\mu_e}{\rho_e} \right) \left( \frac{dv_x}{dr} \right) \bigg|_{r=R} = \frac{\tau_w}{\rho_e} = \left( \frac{1}{8} f v_x^2 \right), \tag{23}$$

where $\tau_w$ is the fluid frictional force per unit area on the pipe and $f$ is the Darcy friction factor which may be calculated using Colebrook's implicit expression as follows

$$\frac{1}{\sqrt{f}} = -2 \log_{10} \left( \frac{\varepsilon / D}{3.7} + \frac{2.51}{\mathrm{Re} \sqrt{f}} \right), \tag{24}$$

where $\varepsilon$, $D$ and $Re$ are respectively, pipe surface roughness, pipe diameter and Reynolds number. The work done due to viscosity effect can be expressed as

$$W_{FV} = \int_0^{2\pi} \int_0^L \left( P_r w + P_x u \right) dx R d\theta. \tag{25}$$

Based on linear potential flow theory, the perturbation pressure induced by fluid can be given as fluid

$$p = \rho_e \left( \frac{\partial \Phi}{\partial t} + v_x \frac{\partial \Phi}{\partial x} \right) \tag{26a}$$

Assuming that there is no cavitation at the fluid-pipe interface, the boundary condition between the pipe wall and the flow is

$$\left( \frac{\partial \Phi}{\partial r} \right)_{r=R} = \left( \frac{\partial w}{\partial t} + v_x \frac{\partial w}{\partial x} \right), \tag{26b}$$

in which $w$ is the transverse deflection of the structure. Using the method of variables separation, the potential function ($\nabla^2\Phi$) in conjunction with boundary condition of (26b) can be solved as

$$\Phi(\mathrm{x}, \mathrm{r}, \theta, \mathrm{t}) = \sum_{m=1}^{M} \sum_{n=0}^{N} \frac{L}{m\pi} \frac{I_n(m\pi r / L)}{I_n^{'}(m\pi R / L)} \left( \frac{\partial w}{\partial t} + v_x \frac{\partial w}{\partial x} \right), \tag{27a}$$

in which I'n is first derivative of $I_n$. Substituting Eq. (27a) into Eq. (26a) yields

$$p = \rho_e \left\{ \sum_{m=1}^{M} \sum_{n=0}^{N} \frac{L}{m\pi} \frac{I_n(m\pi r / L)}{I_n^{'}(m\pi R / L)} \left( \left( \frac{\partial w}{\partial t} \right)^2 + v_x \left( \frac{\partial w}{\partial x} \frac{\partial w}{\partial t} \right) + v_x^2 \left( \frac{\partial w}{\partial x} \right)^2 \right) \right\} \tag{27b}$$

The governing equations of the structure are derived using the Hamilton's principle which is considered as follows

$$\int_0^t \left[ \delta U - \delta K - \delta W_V - \delta W_{FV} - \delta W_{FP} \right] dt = 0. \tag{28}$$

Now, by applying the Hamilton's principle we have

$$\frac{\partial N_{xx}}{\partial x} + \frac{\partial N_{x\theta}}{R\, \partial \theta} = I_0 \frac{\partial^2 u}{\partial t^2}\,, \tag{29}$$

$$\frac{\partial N_{\theta\theta}}{R\, \partial \theta} + \frac{\partial N_{x\theta}}{\partial x} = I_0 \frac{\partial^2 v}{\partial t^2}\,, \tag{30}$$

$$\frac{\partial^2 M_{xx}}{\partial x^2} + \frac{2 \partial^2 M_{x\theta}}{R\, \partial x\, \partial \theta} + \frac{\partial^2 M_{\theta\theta}}{R^2\, \partial \theta^2} - \frac{N_{\theta\theta}}{R} + N_x \frac{\partial^2 w}{\partial x^2} + N_\theta \frac{\partial^2 w}{R^2 \partial \theta^2} + N_{x\theta} \frac{2 \partial^2 w}{R\, \partial x\, \partial \theta} - k_W w + k_g \nabla^2 w - c_v \frac{\partial w}{\partial t} - 2 \frac{\rho_e}{R} U_\tau^2 L - \rho_e U_\tau^2 + \rho_e \left( \frac{\partial \Phi}{\partial t} + v_x \frac{\partial \Phi}{\partial x} \right) = I_0 \frac{\partial^2 w}{\partial t^2}, \tag{31}$$

By integrating the stress-strain relations we have

$$N_{xx}=A_{11}\left(\frac{\partial u}{\partial x}+\frac{1}{2}\left(\frac{\partial w}{\partial x}\right)^2\right)+B_{11}\left(\frac{\partial^2 w}{\partial x^2}\right)+A_{12}\left(\frac{\partial v}{R\partial\theta}+\frac{w}{R}+\frac{1}{2}\left(\frac{\partial w}{R\partial\theta}\right)^2\right)+B_{12}\left(\frac{\partial^2 w}{R^2\partial\theta^2}\right), \quad (32)$$

$$N_{\theta\theta}=A_{12}\left(\frac{\partial u}{\partial x}+\frac{1}{2}\left(\frac{\partial w}{\partial x}\right)^2\right)+B_{12}\left(\frac{\partial^2 w}{\partial x^2}\right)+A_{22}\left(\frac{\partial v}{R\partial\theta}+\frac{w}{R}+\frac{1}{2}\left(\frac{\partial w}{R\partial\theta}\right)^2\right)+B_{22}\left(\frac{\partial^2 w}{R^2\partial\theta^2}\right), \quad (33)$$

$$N_{x\theta}=A_{66}\left(\frac{\partial u}{R\partial\theta}+\frac{\partial v}{\partial x}+\frac{\partial w}{\partial x}\frac{\partial w}{R\partial\theta}\right)+B_{66}\left(\frac{2\partial^2 w}{R\partial\theta\partial x}\right), \quad (34)$$

$$M_{xx}=B_{11}\left(\frac{\partial u}{\partial x}+\frac{1}{2}\left(\frac{\partial w}{\partial x}\right)^2\right)+D_{11}\left(\frac{\partial^2 w}{\partial x^2}\right)+B_{12}\left(\frac{\partial v}{R\partial\theta}+\frac{w}{R}+\frac{1}{2}\left(\frac{\partial w}{R\partial\theta}\right)^2\right)+D_{12}\left(\frac{\partial^2 w}{R^2\partial\theta^2}\right), \quad (35)$$

$$M_{\theta\theta}=B_{12}\left(\frac{\partial u}{\partial x}+\frac{1}{2}\left(\frac{\partial w}{\partial x}\right)^2\right)+D_{12}\left(\frac{\partial^2 w}{\partial x^2}\right)+B_{22}\left(\frac{\partial v}{R\partial\theta}+\frac{w}{R}+\frac{1}{2}\left(\frac{\partial w}{R\partial\theta}\right)^2\right)+D_{22}\left(\frac{\partial^2 w}{R^2\partial\theta^2}\right), \quad (36)$$

$$M_{x\theta}=B_{66}\left(\frac{\partial u}{R\partial\theta}+\frac{\partial v}{\partial x}+\frac{\partial w}{\partial x}\frac{\partial w}{R\partial\theta}\right)+D_{66}\left(\frac{2\partial^2 w}{R\partial\theta\partial x}\right), \quad (37)$$

Where

$$\left(A_{11},A_{12},A_{22},A_{66}\right)=\sum_{k=1}^{N}\int_{z^{(k-1)}}^{z^{(k)}}\left(C_{11},C_{12},C_{22},C_{66}\right)^{(K)}dz, \quad (38a)$$

$$\left(B_{11},B_{12},B_{22},B_{66}\right)=\sum_{k=1}^{N}\int_{z^{(k-1)}}^{z^{(k)}}\left(C_{11},C_{12},C_{22},C_{44},C_{55},C_{66}\right)^{(K)}z\,dz, \quad (38b)$$

$$\left(D_{11},D_{12},D_{22},D_{66}\right)=\sum_{k=1}^{N}\int_{z^{(k-1)}}^{z^{(k)}}\left(C_{11},C_{12},C_{22},C_{44},C_{55},C_{66}\right)^{(K)}z^2dz. \quad (38c)$$

The boundary conditions are taken into account as below

Clamped-Clamped supported

$$\begin{aligned} &w=v=u=0 && @ \quad x=0,L \\ &\frac{\partial w}{\partial x}=0 && @ \quad x=0,L \end{aligned} \quad (39)$$

Simply-Simply supported

$$\begin{aligned} &w=v=\frac{\partial^2 w}{\partial x^2}=0 && @ \quad x=0 \\ &w=v=\frac{\partial^2 w}{\partial x^2}=0 && @ \quad x=L \end{aligned} \quad (40)$$

Clamped-Simply supported

$$\begin{aligned} &w=v=u=\frac{\partial w}{\partial x}=0 && @ \quad x=0 \\ &w=v=\frac{\partial^2 w}{\partial x^2}=0 && @ \quad x=L \end{aligned} \quad (41)$$

## 3. Solution method

Utilizing DQ method, we have (Madani *et al.* (2017), Motezaker and Kolahchi 2017)

$$\frac{d^n f_x(x_i,\theta_j)}{dx^n}=\sum_{k=1}^{N_x}A_{ik}^{(n)}f(x_k,\theta_j) \qquad n=1,\dots,N_x-1. \quad (42)$$

$$\frac{d^m f_y(x_i,\theta_j)}{d\theta^m}=\sum_{l=1}^{N_\theta}B_{jl}^{(m)}f(x_i,\theta_l) \qquad m=1,\dots,N_\theta-1. \quad (43)$$

$$\frac{d^{n+m}f_{xy}(x_i,\theta_j)}{dx^n d\theta^m}=\sum_{k=1}^{N_x}\sum_{l=1}^{N_\theta}A_{ik}^{(n)}B_{jl}^{(m)}f(x_k,\theta_l). \quad (44)$$

where $N_x$ and $N_\Theta$ denote the number of points in x and θ directions, $f\ (x,\ \Theta)$ is the function, and $A_{ik}$, $B_{jl}$ are the weighting coefficients which are in Madani *et al.* (2017). Finally, the motion equations are

$$\left(\left[\underbrace{K_L+K_{NL}}_{K}\right]+\Omega\left[C\right]+\Omega^2\left[M\right]\right)\begin{Bmatrix}\{d_b\}\\\{d_d\}\end{Bmatrix}=\begin{Bmatrix}\{0\}\\\{0\}\end{Bmatrix}, \quad (45)$$

Where $K_L$, $K_{NL}$, $C$, $M$, $d_b$ and $d_d$ represent the linear stiffness matrix, the nonlinear stiffness matrix, the damping matrix, the mass matrix, the boundary points and domain points, respectively.

## 4. Numerical results and discussion

For parametric study, a pipe made from Poly methyl methacrylate (PMMA) is selected with Poisson's ratios of $V_m$=0.34, and Young moduli of $E\_m$=3.52GPa which is reinforced by CNTs with the density of $\rho^{CNT}$=6700 kg/m$^3$, elastic constants of $E_{11}^{CNT}=5.6466$(TPa) and $G_{12}^{CNT}$=1.9455(TPa).

### 4.1 Validation

For validation of our results, the laminated layers, fluid, CNTs and viscoelastic foundation are neglected and frequency of classical cylindrical shells is obtained based on DQM. The structure parameters of the classical shell assumed as *h/R=0.01*, *L/R-20*, *E=210GPa*, *ν=0.3*, *ρ=7840 Kg/m³*. As can be seen from Table 1, the obtained results are close to those expressed in Qu *et al.* (2013) and Tang *et al.* (2016), indicating validation of our work.

Table 1 Validation of present work

| *n* | Qu *et al.* (2013) | Tang *et al.* (2016) | Present |
|---|---|---|---|
| 1 | 0.016103 | 0.016101 | 0.016234 |
| 2 | 0.009382 | 0.011225 | 0.011714 |
| 3 | 0.022105 | 0.022310 | 0.024903 |
| 4 | 0.042095 | 0.042139 | 0.044935 |
| 5 | 0.068008 | 0.068024 | 0.070857 |
| 6 | 0.099730 | 0.099738 | 0.102591 |
| 7 | 0.137239 | 0.137240 | 0.140108 |
| 8 | 0.180528 | 0.180530 | 0.183402 |
| 9 | 0.229594 | 0.229596 | 0.232472 |
| 10 | 0.284436 | 0.284439 | 0.287318 |

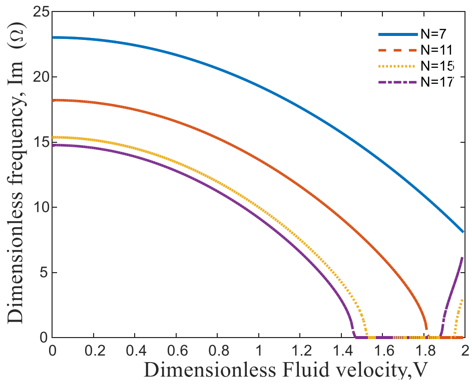


Fig. 2 Convergence of DQM for imaginary part of frequency

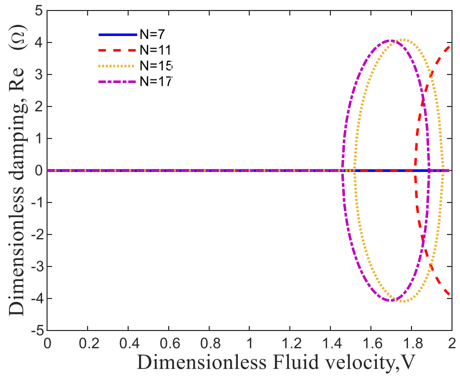


Fig. 3 Convergence of DQM for real part of frequency

### 4.2 The convergence of present method

Figs. 2 and 3 show the convergence and accuracy of DQ method to obtain the imaginary and real part of the dimensionless eigenvalue ($\Omega = \omega R\sqrt{\rho / E}$) against the dimensionless velocity of the fluid ($V = \sqrt{\rho_f / C_{11}}\, v_x$). Chebychev polynomial is used to choose the points in the network about which is explained in part 3. It is clearly seen that there is a fast convergence ratio for the solution method on the imaginary and real part of the dimensionless eigenvalue and the answers reach to a desirable convergence for 17 points. Therefore, the number of the points is considered 17 to extract the results in this research.

### 4.3 Effect of various parameters

Figs. 4 and 5 show the effect of the volume percent of the CNTs on the frequency (Im(Ω)) and system damping (Re(Ω)) according to the fluid velocity ($V$) in a dimensionless manner. As it can be seen, as the velocity of the fluid increases, the imaginary part of the eigenvalue decreases. There is an equal amount with an opposite sign for the real parts of the eigenvalue from this velocity on. Its positive root causes divergence instability in the system. The velocity in which the imaginary and real part of the eigenvalue get zero is called the critical velocity of the fluid. It is observed that the volumetric percent of carbon nanotubes greatly effects on the vibrations and instability of the system. As the volumetric percent of carbon nanotubes increases, frequency (the imaginary part of the eigenvalue)

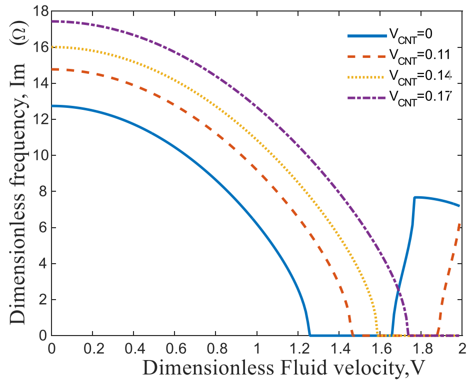


Fig. 4 The effect of volume percent of CNTs on the imaginary part of frequency

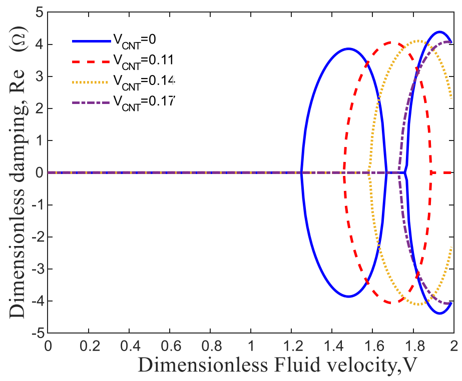


Fig. 5 The effect of volume percent of CNTs on the real part of frequency

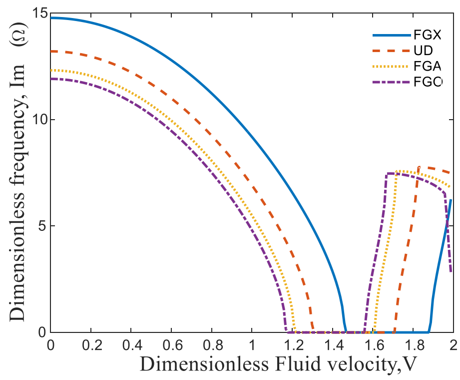


Fig. 6 The effect of distribution of CNTs on the imaginary part of frequency

and critical velocity of the fluid increase due to the increase of construct's hardness by the increase in the volumetric percent of carbon nanotubes.

The effect of distribution of CNTs on the frequency and damping is shown respectively in Figs. 6 and 7 versus the dimensionless fluid velocity. As it can be seen, FGX distribution has maximum frequency and critical fluid velocity. It is since, the distribution of CNTs is out of natural axis.

Figs. 8 and 9 show the effect of lamina layer number on the frequency and damping of the construct based on the fluid velocity, respectively. As it can be seen, there is a direct relationship between the lamina layer number,

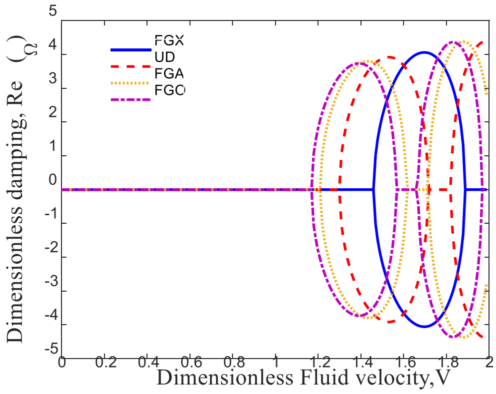


Fig. 7 The effect of distribution of CNTs on the real part of frequency

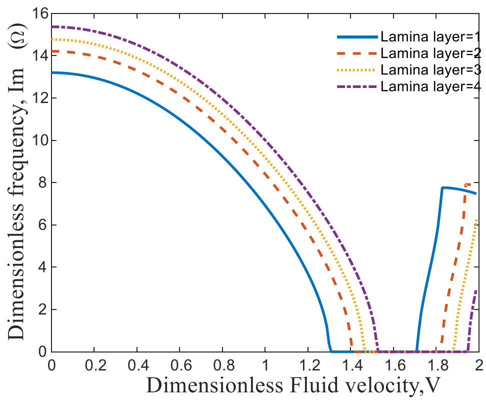


Fig. 8 The effect of lamina layer number on the imaginary part of frequency

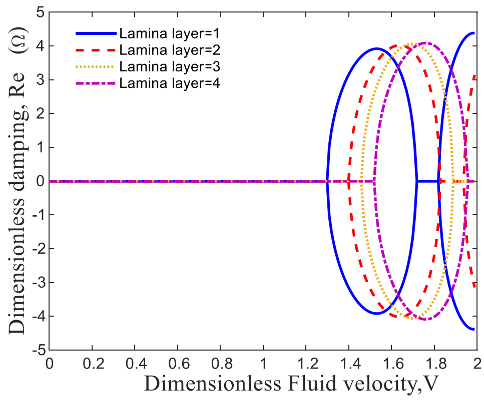


Fig. 9 The effect of lamina layer number on the real part of frequency

frequency changes and critical velocity of the fluid so that as the lamina layer number increases, the frequency and critical velocity of the fluid will increase too.

The effect of length to radius ratio of the pipe on the imaginary and real part of the dimensionless eigenvalue is shown respectively in Figs. (10) and (11) based on the velocity of the dimensionless fluid. It can be understood that the increase in the length to radius ratio of the pipe decreases the frequency and critical velocity of the fluid which is due to the decreasing hardness of the system.

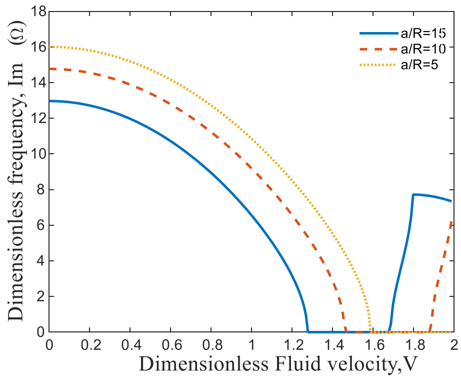


Fig. 10 The effect of length to radius ratio of the pipe on the imaginary part of frequency

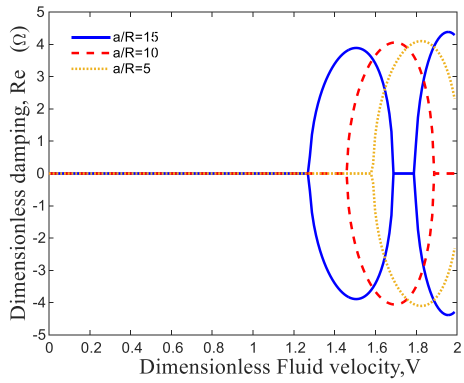


Fig. 11 The effect of length to radius ratio of the pipe on the real part of frequency

The effect of the viscoelastic area is considered as the vertical spring (Winkler), shear layer (Pasternak) and damping ratio. Four aspects are considered to show this effect

- without viscoelastic area
- Visco-Winkler
- Winkler
- Visco- Pasternak
- Pasternak

The effect of viscoelastic medium on the frequency and damping of the construct is shown respectively in Figs. 12 and 13 against the dimensionless velocity of the fluid. It is observed that the bed in which the system is located considerable effects on its vibrations and instability of the system so that if the area is considered viscoelastic, the frequency and the critical velocity of the fluid will increase. The effect of Pasternak area is more than that of Winkler generally since it considers the effect of the shear layer besides the vertical springs.

The imaginary and real parts of the frequency for the eigenvalue are shown in the Figs. (14) and (15) according to the velocity of the fluid for different boundary conditions, respectively. It is observed that the kind of the support severely effects on the instability of the system. As it can be seen, there is a less movement freedom for the system with the clamped support due to its two bounded ends and frequency and critical velocity of fluid is more in it than those in the other supports. Generally, the critical velocity of the fluid is based on the following order in the different

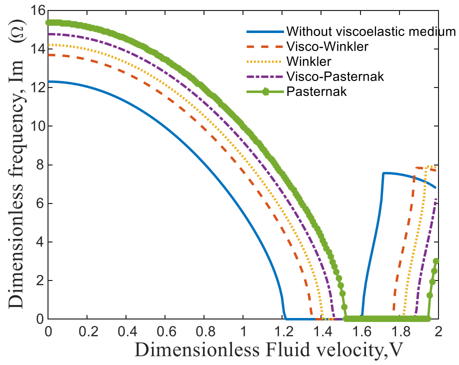


Fig. 12 The effect of viscoelastic medium on the imaginary part of frequency

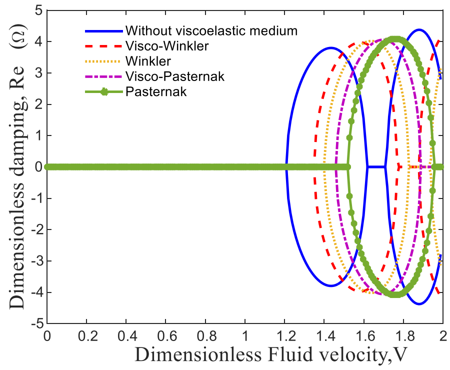


Fig. 13 The effect of viscoelastic medium on the real part of frequency

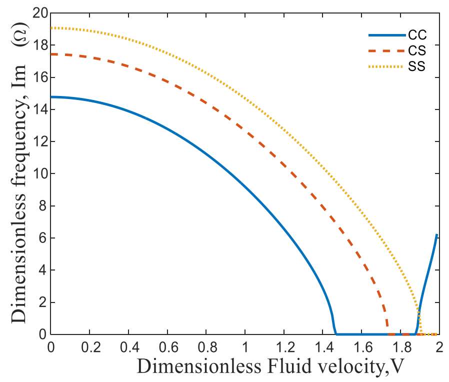


Fig. 14 The effect of different boundary conditions on the imaginary part of frequency

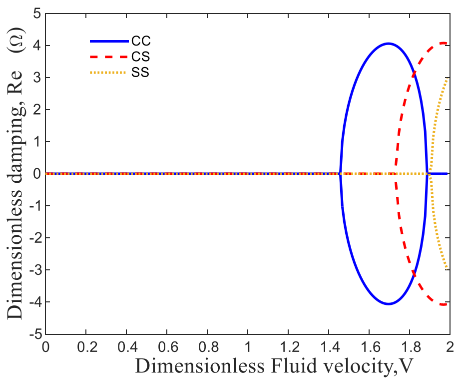


Fig. 15 The effect of different boundary conditions on the real part of frequency

border conditions:
clamped - clamped > clamped - Simple> Simple-Simple

## 5. Conclusions

This research analyzed the vibrations and instability in a nanocomposite laminate pipe reinforced by the carbon nanotube located in a viscoelastic medium with internal turbulent fluid. Mixture model was used to model and determine composite equivalent mechanical properties. Momentum and perturbation equations were applied to extract the force caused by the fluid in the pipe. The motion equations were extracted using nonliclassical theory and Hamilton's principle. This research is aimed to analyze the effect of volumetric percent and distribution of CNTslamina layer number, viscoelastic area, fluid velocity and the geometric parameters of the pipe on the frequency and critical velocity of the fluid. The final results of this research are

- Considering 17 network points leads to the convergence of the results
- As the volumetric percent of CNTs increases, the frequency (the imaginary part of eigenvalue) and critical velocity of the fluid will increase too.
- FGX distribution of CNTs has maximum frequency and critical fluid velocity.
- The increase of length to radius ratio causes the decrease of the frequency and critical velocity of the fluid.
- With enhancing the lamina layer number, the critical fluid velocity increase.
- The effect of Pasternak area is more than that of Winkler since it considers the effect of the shear layer besides that of the vertical spring.

## References

Amabili, M. (2008), "Nonlinear vibrations and stability of shells and plates", New York, Cambridge University Press. New York. U.S.A.

Dai, H.L., Wang, L. and Ni, Q. (2013), "Dynamics of a fluid-conveying pipe composed of two different materials", *Int. J. Eng. Sci*., **73**, 67-76. https://doi.org/10.1016/j.ijengsci.2013.08.008.

Deng, J., Liu, Y., Zhang, Z. and Liu, W. (2017), "Stability analysis of multi-span viscoelastic functionally graded material pipes conveying fluid using a hybrid method", *Europ. J. Mech. A/Solids*, **65**, 257-270. https://doi.org/10.1016/j.euromechsol.2017.04.003.

Ghaitani, M.M. and Majidian, A. (2017), "Frequency and critical fluid velocity analysis of pipes reinforced with FG-CNTs conveying internal flows", *Wind Struct*., **24**(3), 267-285. https://doi.org/10. 12989/Was.2017 .24 .3.267.

He, T. (2015), "Partitioned coupling strategies for fluid-structure interaction with large displacement: Explicit, implicit and semi-implicit schemes", *Wind Struct*., **20**(3), 423-448. https://doi.org/10.12989/was.2015.20.3.423.

Kutin, J. and Bajsić, I. (2014), "Fluid-dynamic loading of pipes conveying fluid with a laminar mean-flow velocity profile", *J. Fluids Struct*., **50**, 171-183. https://doi.org/10.1016/j.jfluidstructs.2014.05.014.

Maalawi, K.Y., Abouel-Fotouh, A.M., Bayoumi, M.El and Yehia, Kh.A.A. (2016), "Design of composite pipes conveying fluid for improved stability characteristics", *Int. J. Appl. Eng. Res*.,**11**(12), 7633-7639.

Madani, H., Hosseini, H. and Shokravi, M. (2017), "Differential cubature method for vibration analysis of embedded FG-CNT-reinforced piezoelectric cylindrical shells subjected to uniform and non-uniform temperature distributions", *Steel Compos. Struct*., **22**(4), 889-913. https://doi.org/10.12989/scs.2016.22.4.889.

Marzani, A., Mazzotti, M., Viola, E., Vittori, P. and Elishakoff, I. (2012), "FEM Formulation for dynamic instability of fluid-conveying pipe on nonuniform elastic foundation", *Mech. Based Des. Struct. Mach*., **40**(1), 83-95. https://doi.org/10.1080/15397734.2011.618443.

Motezaker, M. and Kolahchi, R. (2017), "Seismic response of SiO2 nanoparticles-reinforced concrete pipes based on DQ and newmark methods", *Comput. Concrete*, **19**(6), 745-753. https://doi.org/10.12989/cac.2017.19.6.745.

Ni, Q., Luo, Y., Li, M. and Yan, H. (2017), "Natural frequency and stability analysis of a pipe conveying fluid with axially moving supports immersed in fluid", *J. Sound Vib*., **403**, 173-189. https://doi.org/10.1016/j.jsv.2017.05.023.

Ni, Q., Zhang, Z.L. and Wang, L. (2011), "Application of the differential transformation method to vibration analysis of pipes conveying fluid", *Appl. Math. Comput*., **217**(16), 7028-7038. https://doi.org/10.1016/j.amc.2011.01.116.

Qian, Q., Wang, L. and Ni, Q. (2009), "Instability of simply supported pipes conveying fluid under thermal loads", *Mech. Res. Commun*., **36**(3), 413-417. https://doi.org/10.1016/j.mechrescom.2008.09.011.

Qu, Y., Hua, H. and Meng, G. (2013) "A domain decomposition approach for vibration analysis of isotropic and composite cylindrical shells with arbitrary boundaries", *Compos. Struct*., **95**, 307-321. https://doi.org/10.1016/j.compstruct.2012.06.022.

Reddy, J.N. (2004), "Mechanics of laminated composite plates and shells", CRC press, Washington. U.S.A.

Rivero-Rodriguez, J. and Pérez-Saborid, M. (2015), "Numerical investigation of the influence of gravity on flutter of cantilevered pipes conveying fluid", *J. Fluids Struct*., **55**, 106-121. https://doi.org/10.1016/j.jfluidstructs.2015.02.009.

Ryu, B.J., Ryu, S.U., Kim, G.H. and Yim, K.B. (2004), "Vibration and dynamic stability of pipes conveying fluid on elastic foundations", *KSME Int. J*., **18**(12), 2148-2157. https://doi.org/10.1007/BF02990219.

Sun, F.J. and Gu, M. (2014), "A numerical solution to fluid-structure interaction of membrane structures under wind action", *Wind Struct*., **19**(1), 35-58. https://doi.org/10.12989/was.2014.19.1.035.

Tang, D., Wu, G., Yao, X., and Wang, Ch. (2016), "Free vibration analysis of circular cylindrical shells with arbitrary boundary conditions by the method of reverberation-ray matrix", *Shock Vib*., 3814693, https://doi.org/10.1155/2016/3814693.

Texier, B.D. and Dorbolo, S. (2015), "Deformations of an elastic pipe submitted to gravity and internal fluid flow", *J. Fluids Struct*., **55**, 364-371. https://doi.org/10.1016/j.jfluidstructs.2015.03.010.

Wang, L. (2012), "Flutter instability of supported pipes conveying fluid subjected to distributed follower forces", *Acta Mech. Solida. Sin*., **25**(1), 46-52. https://doi.org/10.1016/S0894-9166(12)60005-6.

*CC*